Grain Settlement and Fluid Flow Cause the Earthquake Liquefaction of Sand

Daniel L. Lakeland
University of Southern California

Amy Rechenmacher
University of Southern California

Roger Ghanem
University of Southern California

July 10, 2013

Abstract

When loosely packed water-saturated granular soils such as sands are subject to strong earthquake shaking they may liquefy, causing large deformations with great destructive power. The phenomenon is quite general and occurs in any fluid saturated granular material and is a consequence of the transfer of stress from inter-grain contacts to water pressure. In modern geotechnical practice soil liquefaction is commonly considered to be an "undrained" phenomenon; pressure is thought to be generated because earthquake deformations are too quick to allow fluid flow which enables water depressurization. Here we show via a first principles analysis that liquefaction is not a strictly undrained process; and in fact it is the interplay between grain rearrangement, fluid migration, and changes in permeability which cause the loss of strength observed in so many destructive earthquake events around the world. The results call into question many of the common laboratory and field methods of evaluating the liquefaction resistance of soil and indicate new directions for the field, laboratory, and scale-model study of this important phenomenon.

Background

The general phenomenon of the liquefaction of granular materials is applicable to a wide variety of grains and fluids. Here, we focus on one of the most important aspects of this phenomenon, namely the earthquake induced liquefaction of sand near the ground surface. Our analysis uses a nondimensional formulation and asymptotic analysis which is adapted to the first few tens of meters of soil where the interplay of gravity, grain rearrangement, water compressibility, and water flow combine to cause these destructive events.

In the Geotechnical Engineering field, soil liquefaction is commonly understood as a consequence of water pressure buildup due to rapid squeezing of pore spaces, without sufficient time for water to flow through the grains and drain the pressure, eg. [1, 2, 3]. When grains are loosely packed, during earthquake motion the tendency is for soil grains to move closer together, squeezing the water and rapidly increasing the pressure due to the high bulk modulus of water. Taken across a thin horizontal section of the soil, the total force is the sum of the contact forces between grains, and the water pressure times the area of the cross section. This "total stress" minus the water pressure is the so called "effective stress", commonly used in geotechnical analysis [3], which is a measure of the contribution of grain-grain interactions in the soil. If the contact forces drop to zero, then the water pressure carries the entire normal stress, and shear stresses induce flow in the manner of a viscous fluid.

The goal of liquefaction assessment up to now has been to determine how the water pressure in the soil will change during cyclic loading. The methodology employed has primarily been to build models based on the results of laboratory triaxial, hollow cylindrical, and simple shear tests, as well as more extensive physical centrifuge models. Laboratory tests use samples of sand typically around 10 to 20 cm in characteristic size. The sand is surrounded by an impermeable, flexible membrane to trap the pore water, and the entire sample is contained in a pressurized vessel to simulate the overall pressure conditions in the ground. Cyclic loading of various forms is applied and the total and effective stress states, and evolution of pore water pressure are tracked through the cycling. These experiments have been extensively performed. To complement these small laboratory scale tests, extensive physical modeling in various types of geotechnical centrifuge apparatus have been carried out. These tests use centrifugal acceleration to model the stresses induced in deposits of soil that are 10 to 100 times deeper than the model scale and allow full 3 dimensional geometries to be simulated without the ambiguity of numerical simulations of complex soil materials. Combined with these physical observations, engineers have employed correlations with observed field conditions in post-seismic investigations. An overview of the current state of liquefaction research may be found in [1].

Implicit in the use of small laboratory samples with impermeable membranes, and explicit in many textbook definitions of liquefaction, is the assumption that during the earthquake there is no significant water flow or change in water volume, which is known as the "undrained" condition (cf. [2, 3]). The assumption that soil liquefaction occurs under undrained conditions has lead to extensive research into undrained tabletop experiments such as triaxial and simple shear tests, with several methods suggested to overcome the small volume changes allowed by the compliance of the rubber membrane [4]. Although centrifuge and laboratory test data have long shown that water migration can occur [5, 6], these situations have been treated as if they were exceptions to the normal situation of undrained pore pressure increase.

With the advent of large computing power, more recent studies of liquefaction phenomena have used discrete element models (DEM) which operate at the grain scale, and calculate the equations of motion for thousands of individually

tracked cylindrical or spherical grains. In [7] a 2D DEM model was coupled to a continuum model for fluid flow, and the interactions of grains and fluid were calculated for a sample of a few thousand grains. Their conditions are typical of 200m to 2km deep thin deposits sheared at ord(1) to ord(10) m/s [1] which is relevant for fault gouge conditions. Holding boundary conditions of their sample at either zero fluid mass flow, or constant fluid pressure, they were able to observe liquefaction for both dense and loose sheared assemblies under drained and undrained conditions. While their method is in principle applicable to a wide variety of situations, computing the interactions of large deposits of sand over meters or tens of meters would be computationally prohibitive. Their model does show, however, that our understanding of even tabletop sized experiments may be flawed, as they observe liquefaction under all conditions in assemblies whose bulk density was either relatively loose or relatively dense. In an earlier paper, [8] derived a nondimensional continuum equation for dynamic fluid flow which is valid for mesoscopic scales and based on conservation of mass together with Darcy's law. Their equation provides much of what is required to analyze a realistic soil deposit, though they explicitly neglect certain aspects such as thermal heating and they do not extensively analyze the equation in the context of typical near-surface liquefaction conditions.

In this paper, we analyze the liquefaction of saturated sandy and silty soils in the first ord(10) meters below the ground where initial water pressures are within a few atmospheres of the total vertical stress. Our method is to derive a one dimensional equation for fluid flow in the vertical direction based on the assumptions of mass conservation and Darcy's law for fluid flow through porous media in a manner very similar to [8]. Although the same derivation can be trivially extended to 3D mathematically, it provides no additional qualitative understanding for the main point of this study, which is that fluid flow and soil inhomogeneity are of critical importance in the liquefaction phenomenon.

By treating a comprehensive set of dependencies including temperature effects and the compressibility of water potentially containing some small quantity of gas such as arising from organic processes or dissolved gasses, we arrive at a very general result which leaves no further degrees of freedom that could be expected to contribute significantly to water pressurization in these soils. By nondimensionalizing the model using a distinguished limit [9] we focus attention on the relative size of the various effects that can cause fluid pressurization and transfer of stress from soil particles to the water under the relevant circumstances. By showing that heating and compressibility of water are both perturbation effects, our results clarify that grains collapsing into denser arrangements pressurizes the fluid, and that pressure diffusion can not be neglected in the liquefaction process. Indeed, we show that for loose sands diffusion is equally important to densification on timescales significantly shorter than the duration of an earthquake.

For layered deposits or samples with spatially varying permeability, gradi-

[1] Note on our use of asymptotic notation: $x = \mathrm{O}(y)$ means that $|x/y| < C$ for some positive constant C which is expected to be not extremely large, $x = \mathrm{ord}(y)$ means $|x/y|$ and $|y/x|$ should both be treated as close to 1 and $x = \mathrm{o}(y)$ means $|x/y|$ is negligibly small.

ents in the permeability field are critical in determining where liquefaction onset might occur. Though this has been shown in a variety of experiments, this has never been explicitly analyzed mathematically to determine how important this effect is in general. For example, small regions of soil with permeability lower than sand will result in large pressure gradients so that the small layer responds on similar time scales as the surrounding sand. By a simple rescaling argument, we can see that in extensive silt deposits, gravitational effects, and pressure diffusion through flow become less important on the earthquake duration timescale, and instead pressure change is more directly related to contractive grain motion and heating. Therefore, our model explains the dominant effects in a range of conditions from very low permeability soils typical of silts, through sands, and even in the case of high permeability gravels where diffusion is more dominant. One value of the model is that it predicts certain new features, such as large settlements together with bulk fluid flow to the surface in loose high permeability deposits, and also suggests a new mechanism of liquefaction potentially mediated by heating within silts even if the silt's initial density is such that sustained contractive loading does not occur. We compute solutions for several example scenarios that mimic the observed dynamics in tabletop [6, 10] and centrifuge experiments [5]

Based on the results of these analyses, we believe that liquefaction evaluation approaches should explicitly acknowledge the importance of fluid flow. Future efforts should be placed on evaluating permeability, porosity, and the energetic potential for earthquake-induced porosity changes over entire deposits of soil, not mainly the existence of layers of loose sands and a notional "resistance to liquefaction" based on shear stresses, as is common in current Geotechnical Engineering practice [11, 12].

In addition to a description of the fluid flow, the prediction of the grain motions is of great interest, as it is a driving force for the fluid pressurization and migration. At present the authors are unaware of any continuum model which could reliably substitute for the results of fully coupled DEM and yet be computationally tractable for large scales of spatially variable soil deposits. Because of this limitation, we apply an assumed grain deformation, usually a constant in space, and investigate the predicted results in terms of the induced fluid flow.

Model Construction

We assume a horizontally layered deposit of soil, and a vertical coordinate axis pointing upward with zero reference point at a deep impermeable layer below the region of interest. We choose this coordinate system rather than one oriented downward from the ground surface since the ground surface may settle downward. We are interested in the first few tens of meters below the ground surface, as this is where small pore volume strains can produce changes in water pressure that can easily produce a zero effective stress condition. We consider a thin horizontal slice of this material with cross sectional area A which is very

large compared with the typical size of a grain, and thickness dz which is on the order of several grain diameters. For the saturated sands we consider, the fluid in our differential volume at pressure P and density ρ fills the inter-grain spaces whose volume is $V_f = \phi A dz$, where ϕ is the bulk porosity (the fraction of total volume occupied by pore space). Since the bulk modulus of the grains is typically an order of magnitude higher than that of the fluid, which is already quite high, we assume that the individual grains do not compress by any appreciable amount. However, grain rearrangement can cause changes in porosity.

While the usual assumption in liquefaction research is that fluid flow does not occur on the time scale of the earthquake, we instead model the rate of change of fluid mass within the volume by examining the difference in the fluid flux out of the top surface and into the bottom surface. We can estimate the fluid flow rate v_f relative to the grains moving at velocity v_g using Darcy's law $v_f - v_g = -\frac{k_d}{\mu}\frac{\partial P}{\partial z}$, where k_d is permeability and μ is the fluid viscosity. Darcy's law has been established to give an accurate effective fluid flow velocity v_f which gives the proper volumetric flow rate when multiplied by the total cross sectional area of a representative volume. This equation represents an approximation of the full fluid flow equation when only viscous effects and pressure gradients dominate.

Assuming that the horizontal slice can be made thin enough relative to the length scale over which fluid velocity varies, the resulting differential equation for change in fluid mass within the differential slice is:

$$\frac{d}{dt}\left(\rho\phi A dz\right) dt = -\frac{\partial}{\partial z}\left(A\rho\left(-\frac{k_d}{\mu}\frac{\partial P}{\partial z} + v_g\right) dt\right) dz - \Delta M_{\text{static}} \tag{1}$$

Here the left hand side expresses the change in a short time dt of the total fluid mass in the slice. The right hand side expresses the difference in fluid mass flux which is moving relative to the grains at velocity $\frac{k_d}{\mu}\frac{\partial P}{\partial z}$. To get the absolute velocity in a Newtonian reference frame we add v_g.

The term ΔM_{static} is a correction necessary to account for the fact that there is no change in the slice's water mass when static gravitational conditions apply. For example, due to gravity there is a static pressure gradient. Also, the permeability changes with depth, and water density changes minutely with depth. Setting the left side of the equation equal to zero when static gravitational conditions apply and solving for the correction gives

$$\Delta M_{\text{static}} = \frac{\rho^2 g A}{\mu}\left(\frac{g k_d \rho_0}{K_B} - \frac{k_d}{\rho}\frac{d\rho}{dz} - \frac{\partial k_d}{\partial z}\right) dt dz \tag{2}$$

In equations (1) and (2), for a vertical cartesian axis z, A, dz, and dt are constant, k_d depends on location z, μ depends on temperature T, ρ is determined from P and T using the state equation, and P, T and ϕ depend on time t and position z. Because liquefaction of soils takes place over a very small range of fluid density and temperature conditions, we can use a linear Taylor expansion of the state equation for water to eliminate the density ρ from the equation by

solving for it in terms of pressure and temperature. The Taylor expanded state equation is:

$$P(\rho, T) = P_0 + \frac{K_B}{\rho_0}(\rho - \rho_0) + K_B\alpha(T - T_0) \tag{3}$$

Where P_0, ρ_0 and T_0 are reference pressure, density, and temperature levels for the water, K_B is the bulk modulus of water ($-V\frac{\partial P}{\partial V}_T$), α is the coefficient of volumetric thermal expansion ($\frac{1}{V}\frac{\partial V}{\partial T}_P$), and ρ and T are the actual density and temperature. The temperature dependence can be derived from allowing a volume of water to be heated and expand under constant pressure, and then be squeezed back to its original volume at constant temperature. For our purposes we neglect the very small difference between the adiabatic and isothermal bulk modulus of water.

Note that we may compensate for the presence of a small fraction of the voids containing gas by adjusting K_B. If a volume of water contains small bubbles occupying a small fraction ϵ of the volume, then we can approximate the compressibility ($1/K_B$) using $V = V_W + V_g$ and $1/K_B = -\frac{1}{V}\frac{\partial V}{\partial P}$ together with the state equation $PV = KT$ for an ideal gas and the taylor series state equation for the liquid $V_l = V_0(1 - (P - P_0)/K_B)$. Assuming isothermal gas compression due to the thermal equilibrium with the water, $V_g = V_0P_0/P$, evaluating the derivative at P_0, we get:

$$\frac{P_0}{K_{B_{\text{mix}}}} = \epsilon\left(1 - \frac{P_0}{K_B}\right) + \frac{P_0}{K_B}$$

where K_B is the bulk modulus of water, and P_0 is the reference pressure, which we take as the initial absolute pressure of the mixture. This is a strong function of ϵ since P_0/K_B is small for atmospheric scale pressures. This may be relevant in situations involving gas bubbles formed by biological organisms or recent rains bearing an excess of dissolved gas, or in tidal areas where fluxes of water and gas bubbles are large.

Since we used the state equation involving P and T to eliminate ρ, our equation now includes the temperature T and in expanded form will include both $\frac{\partial T}{\partial t}$ and $\frac{\partial T}{\partial z}$. We use the following heat equation for a flowing fluid to relate these quantities:

$$\frac{dT}{dt} + \frac{\partial T}{\partial z}v = \frac{1}{\rho_{\text{avg}}c_v}\left(k_T\frac{\partial^2 T}{\partial z^2} + T\frac{\partial S}{\partial t}_Q\right) \tag{4}$$

In (4) c_v is a bulk averaged specific heat capacity, ρ_{avg} is the bulk average density, k_T is the effective thermal conductivity, and $\frac{\partial S}{\partial t}_Q$ is the change in entropy density due to heat generation.

In addition, the conservation of grain mass was used to replace $\frac{\partial v_g}{\partial z}$ with a term involving $\frac{\partial \phi}{\partial t}$ and a convective term involving v_g, which will become a perturbation due to the small settlement velocities.

$$\frac{\partial(1-\phi)}{\partial t} = -\frac{\partial(1-\phi)v_g}{\partial z} \rightarrow \frac{\partial v_g}{\partial z} = \frac{1}{(1-\phi)}\left(\frac{\partial \phi}{\partial z}v_g + \frac{\partial \phi}{\partial t}\right) \tag{5}$$

In this form, these equations are not yet useful for analysis and calculation, as within each derivative there are multiple variables whose values are dependent on time or position. Our next task will be to expand the fluid equation (1) through the comprehensive application of the chain rule, so we can arrive at an equation for the rate of change of pressure $\frac{\partial P}{\partial t}$ and then make this equation dimensionless to help evaluate the relative importance of various terms.

We employed the freely available Maxima computer algebra system [13] to calculate the expanded version of equation 1. When expanded as a polynomial in the important variables and derivatives the equation had 33 terms each of which had multi-term coefficients. Maxima's textual representation of the full equation was approximately 25 times as long as the representation of our fully simplified equation and thus is not displayed here. This full equation includes many terms whose effects are orders of magnitude smaller than the main effects and are therefore negligible. By identifying and dropping negligible terms we arrive at a simplified "full" equation which captures all of the dynamics of interest including first order perturbations (equation 14 is the fully analyzed dimensionless version below).

In order to arrive at the simplified equation, we needed to understand the dominant balances of effects and identify the negligible terms. To do this a proper nondimensionalization is required. The choice of the characteristic scales for nondimensionalization is one of the critical aspects of our analysis, since it focuses the equation on the specific situations of interest.

To focus our understanding on geotechnically relevant scales, we chose scales for P, k_d and ϕ by reference to the situation in the first several meters of sandy soil, where $P/P_0 = \mathrm{O}(1)$ throughout. We introduce k_{d0} which represents a typical order of magnitude for permeability of moderately coarse loose sands, such that the permeability range for most sands falls within about a factor of 4 of this value. We also introduce ϕ_0 which represents a typical value for porosity in a loose sand. General sands are between about 70% and 110% of this ϕ value. These values were chosen by reference to tables given in [14].

$$\begin{aligned} P_0 = P_{\mathrm{atm}} &= 100\,\mathrm{kPa} \\ k_{d0} &= 1.5 \times 10^{-10}\,\mathrm{m}^2 \\ \phi_0 &= 0.44 \end{aligned} \tag{6}$$

We wrote equations for the dimensional variables in terms of nondimensional

"primed" or "hatted" variables as follows:

$$\begin{aligned}
\phi &= \phi_0 \left(1 + \frac{\Delta\phi}{\phi_0}\,\phi'\right) \\
\hat{\phi} &= \phi/\phi_0 \\
P &= P_0 + P_0 P' \\
z &= \Delta z\, z' \\
k_d &= k_{d0}\, k'_d \\
t &= \Delta t\, t' \\
v_g &= \frac{6\Delta\phi\Delta z}{\Delta t} v'_g \\
S &= \Delta S\, S' \\
T &= T_0 \left(1 + \frac{\Delta S}{C_{v0}}\, T'\right)
\end{aligned} \tag{7}$$

Here $C_{v0} \approx 1594\,\mathrm{J/kg/K}$ represents a mass weighted average of the specific heat capacity of grains and water. We took numerical values as $C_{vwat} = 4156.7\,\mathrm{J/kg/K}$ and $C_{vgr} = 835\,\mathrm{J/kg/K}$. We then substituted these expressions into the expanded dimensional form of equation 1 and solved for the dimensionless $\frac{\partial P'}{\partial t'}$.

The variable ϕ' is our new dynamic variable related to porosity that represents normalized dynamic fluctuations in ϕ contributing on the order of $\frac{\Delta\phi}{\phi_0} \ll 1$, whereas $\hat{\phi}$ represents a normalized value of ϕ as a fraction of its typical size, a value which changes little during the event due to the large separation of the scales of ϕ' and $\hat{\phi}$. The scaling of dimensional velocity v_g was chosen so that 1 unit of v'_g represents a ground settlement of about 10 cm during a 30 s earthquake after computing $\Delta\phi$ as described below.

The remaining scale constants Δz, Δt, ΔS and $\Delta\phi$ can be chosen arbitrarily, however the situation with the maximal interplay of different effects is the so called distinguished limit [9], where all of the relevant terms in the equation have coefficient equal to 1 under typical conditions so that one unit of change in any variable or derivative induces the same size of effect compared to changes of any other variable or derivative. By calculating our scale factors to force the equation into this form, we identify the regime in which maximal interplay occurs.

To calculate the scale constants, we evaluate the coefficients under the conditions $k'_d = 1$ and $\phi = \phi_0$ as representative of typical conditions, and then require the important terms $\frac{\partial^2 P'}{\partial z'^2}$, $\frac{\partial \phi'}{\partial t'}$, and $\frac{\partial P'}{\partial z'}\frac{\partial k'_d}{\partial z'}$ which represent the effect of pressure diffusion, grain skeleton contraction, and spatial variability in permeability respectively to have coefficients equal to 1. In addition we require the initial dimensionless gravitational static pressure gradient to be 1. These four equations are sufficient to constrain the values of Δz, Δt, ΔS and $\Delta\phi$ and we solve for them as follows:

$$
\begin{aligned}
\Delta z &= P_0/\rho_0 g && \approx 10\,\mathrm{m} \\
\Delta t &= \frac{\phi_0 \mu P_0^2}{g^2 k_{d0} K_B \rho_0^2} && \approx 0.14\,\mathrm{s} \\
\Delta S &= \frac{C_{v0} P_0 \gamma_S}{\alpha K_B T_0} && \approx 6.0 \times 10^{-3}\,\mathrm{J/kg/K}\,(\gamma_S = 1) \\
\Delta \phi &= \frac{\phi_0(1-\phi_0)}{(2-\phi_0)} \frac{P_0}{K_B} && \approx 7.2 \times 10^{-6}
\end{aligned}
\tag{8}
$$

Clearly our assumption that diffusion, contraction, and permeability variation are all important in realistic flow regimes is validated by the magnitude of these scale constants. Δt is small compared to an earthquake duration of 30 s, the length scale is $O(1)$ relative to the size of deposits of interest, and $\Delta\phi$ is a reasonably achievable fluctuation in ϕ. The fact that Δt is small compared to the earthquake duration means that a near-equilibrium approximation of the flow should be valid for predicting the pressure field at the end of earthquake shaking.

Note in the above scales we have left γ_S as a nondimensional parameter which measures the fraction of the "distinguished limit" level of heating which actually occurs in practice. If $\gamma_S = 1$, then this implies a characteristic temperature change rate of 1.05 K/s which for a 30 s earthquake implies 32 K temperature change, a clearly untenable quantity: the sand would be scalding hot, a phenomenon not reported previously. The distinguished limit with heating is therefore more relevant for some mechanical apparatus in which external heating is applied, or perhaps a geothermal or fault gouge condition. However, as pointed out by [15] and verified in field observations by [16], dissipated mechanical energy is highly correlated with water pressure development. Clearly, the wave energy is used by the grains as activation energy for rearrangement, and this process is irreversible and must produce *some* heat. To estimate the actual scale of heating within the soil, and constrain γ_S, we made reference to the entropy generated by the flow of water through a characteristic soil under a characteristic pressure gradient. We calculate this entropy scale by assuming that the water flows horizontally for Δt seconds through a constant pressure gradient $P_0/\Delta z$ at a velocity given by Darcy's law, and the work done by the pressure field (the change in enthalpy) is completely converted to entropy at temperature T_0, via drag from the particles:

$$
\begin{aligned}
\gamma_{S\min} &= \left(\frac{P_0}{\Delta z}\right)\left(\frac{k_{d0}}{\mu}\frac{P_0}{\Delta z}\right)\frac{\Delta t}{T_0 \rho_w}\left(\frac{1}{\Delta S_{\gamma_S=1}}\right) \\
&= \frac{\alpha \phi_0 P_{\mathrm{atm}}}{C_{v0}\rho_w} \\
&\approx 6 \times 10^{-6}
\end{aligned}
\tag{9}
$$

This is a lower bound for the relative entropy generation in the soil as it does not include any effect of the grain motion. To bound the range of reasonable values for γ_S we assumed that during a 20 second earthquake soil temperature

should not change more than ord(1) K since an order of magnitude more would not be ignorable, and temperature must change at least ord(10^{-4}) K due to the flow entropy calculated above. As a representative value, we therefore chose $\gamma_S \approx 5 \times 10^{-3}$ under the assumption that the grain motion contributes significantly to entropy production but that the temperature change is still a fraction of a Kelvin. The implied characteristic change in temperature for the soil overall is 0.24 K in 30 s. This would seem to be a large fraction of the amount that could occur while still being neglected in most field or laboratory experiments. Even if the true value is an order of magnitude larger than this, our treatment of the effect as a small perturbation will remain valid.

After nondimensionalizing, we replaced each of four important nondimensional groups with a single nondimensional symbol for each group as follows:

$$\gamma_{\text{vol}} = \frac{P_{\text{atm}}}{K_B} \tag{10}$$

$$\gamma_{\mu_T} = \frac{1}{\alpha\mu}\frac{d\mu}{dT} \tag{11}$$

$$G_{\text{gr}} = \rho_{\text{grain}}/\rho_0 \tag{12}$$

$$\beta(\hat{\phi}) = \frac{1 + \frac{1}{(1-\phi_0\hat{\phi})}}{\hat{\phi}\left(1 + \frac{1}{(1-\phi_0)}\right)} \tag{13}$$

Above, γ_{vol} expresses the compressibility of water in terms of the volumetric strain required to generate a characteristic unit of pressure, $\gamma_{\mu T}$ represents fractional change in viscosity for a nondimensional unit of temperature change, and G_{gr} is the relative density of grains to water, typically about 2.6 to 2.7; here, we have used 2.655. β is the local nondimensional bulk modulus of the mixture, measuring the nondimensional water pressure change per change in ϕ' and is a function of the local $\hat{\phi}$ value ranging in practice between about 1 and 2 for realistic values of $\hat{\phi} \in [0.5, 1.1]$. For important constants related to water, we used the values of density, heat capacity, viscosity, and other important properties available online from the NIST database of the properties of water for a reference pressure of P=100kPa and temperature T=293.15K ($20°C$)[17].

By construction, for typical conditions of soil liquefaction all the variables and their derivatives are O(1) so that the relative size of each term is determined from its coefficient. In certain conditions these assumptions are violated, such as near sudden transitions in permeability. To eliminate negligible terms we performed an asymptotic analysis of the equation, neglecting terms with very small coefficients except for the first order dominant perturbations. Since $\gamma_{\text{vol}} \ll 1$, we took a first order Taylor series about 0 for this parameter eliminating many small terms. Terms involving the diffusion of temperature had tiny coefficients and were dropped. Finally, an asymptotic analysis of the remaining compressibility and heating related terms using the method of multiple scales identified the leading order terms related to these two processes. Retained perturbation terms are relevant only near large gradients in permeability, large gradients in pressure, or extremely low permeability regions. The final equation is:

$$\begin{aligned}\frac{dP'}{dt'} &= -\beta\left(\hat{\phi}\right)\frac{\partial\phi'}{\partial t'} \\ &+ \frac{1}{\hat{\phi}}\left(k'_d\frac{\partial^2 P'}{\partial z'^2} + \frac{\partial k'_d}{\partial z'}\left(\frac{\partial P'}{\partial z'}+1\right)\right) \\ &+ \frac{\frac{\partial S'}{\partial t'}\gamma_S}{C'_v\left(\hat{\phi}\right)} \\ &+ \gamma_{\text{vol}}\left(-\beta\left(\hat{\phi}\right)\frac{\partial\phi'}{\partial t'}P' + \frac{1}{\hat{\phi}}\left(-k'_d\frac{\partial P'}{\partial z'}\frac{\partial T'}{\partial z'}\gamma_S\,\gamma_{\mu_T} + k'_d\,P'\frac{\partial^2 P'}{\partial z'^2} + k'_d\left(\frac{\partial P'}{\partial z'}\right)^2 + \frac{\partial k'_d}{\partial z'}P'\frac{\partial P'}{\partial z'}\right)\right)\end{aligned} \tag{14}$$

Equation (14) describes all relevant features of our model including small first order perturbations due to water compressibility and thermal effects. In this equation $C'_v(\hat{\phi})$ is the nondimensional relative heat capacity as a fraction of C_{v0} which changes due to spatial changes in porosity, and $\beta(\hat{\phi})$ is the nondimensional bulk modulus of the mixture defined above (equation 13). In equation (14) the eliminated terms all had coefficients smaller than about 10^{-9}.

It is at this point that the assumption of "fluid incompressibility," which is often invoked from the beginning in soil mechanics, can be applied in a rational manner by taking a limit as $\gamma_{\text{vol}} \to 0$. This assumption is a helpful one and justified for most purposes involving soil liquefaction. The primary conditions in which compressibility can become significant are high pressure gradients in low permeability soils, such as at the center of thin layers of silt, the spatial regions where these conditions occur are necessarily small as if $|\frac{\partial k_d}{\partial z}|$ is large then k_d can not remain small. Thus the term multiplied by γ_{vol} is dropped, and the resulting simplified equation is:

$$\begin{aligned}\frac{dP'}{dt'} &= -\beta\left(\hat{\phi}\right)\frac{\partial\phi'}{\partial t'} \\ &+ \frac{1}{\hat{\phi}}\left(k'_d\frac{\partial^2 P'}{\partial z'^2} + \frac{\partial k'_d}{\partial z'}\left(\frac{\partial P'}{\partial z'}+1\right)\right) \\ &+ \frac{\frac{\partial S'}{\partial t'}\gamma_S}{C'_v\left(\hat{\phi}\right)}\end{aligned} \tag{15}$$

Qualitative Results

Some basic simplified models for the qualitative behavior expected from these equations are now considered. First, recall that the characteristic time scale $\Delta t \approx 0.14\,\text{s}$ for this system is smaller than the time scale for a typical earthquake period of about 1 s and much smaller than a typical earthquake duration $> 10\,\text{s}$. This means that within the loose sands that are traditionally thought to be the main risk for liquefaction, the pressure field remains close to equilibrium throughout the earthquake due to pressure diffusion effects, since any ord(1)

imbalance in any of the terms of the equation would induce ord(1) bars of pressure change over 0.14 s, a timescale shorter than the duration of a single loading cycle, returning the system rapidly to near equilibrium. Even for fine sands where $k_d \sim k_{d0}/20$ the time scale would be approximately the same order as a single loading cycle and significantly shorter than typical earthquake duration. Only when permeability is similar to the permeability of silts $k_{d0}/1000$ can we assume that the pressure diffusion time is long compared to earthquake duration so that "undrained" conditions might be a reasonable approximation. Even in these cases, as we shall see in examples, when a silt layer is small and in contact with a sandy layer, very high curvature of the pressure field and large gradients generated near these interfaces can begin to equalize the response time between the sand and the silt. Clearly flow can not be neglected in earthquake liquefaction of sand. To support this hypothesis with physical data, we can reference for example the centrifuge model B of [5]. In this test, a sand layer is overlain by silt. Shaking starts at approximately 2 seconds, and lasts until approximately 12 seconds. By 4 seconds the sand has come to a locally time-averaged equilibrium with a fast oscillation superimposed due to continued shaking, and the silt has a similar if slightly slower response, achieving a locally time-averaged equilibrium at approximately 10 seconds which is before the end of shaking at 12 seconds (times given in prototype dimension). Failure of the silt layer via a sand-boil is not seen until 50 seconds. An equilibrium solution of the flow equations based on time-averaged rate of change of porosity could be expected to be quite accurate even before the shaking stopped, if the loading were taken to be the time average of the actual loading over a few seconds.

Because of this near-equilibrium state, we can approximate the pressure field at liquefaction by solving the steady state equation for the forcing $\frac{\partial \phi'}{\partial t'}$ required to make the water pressure field tangent to the total vertical stress. Once we have this solution we can find the location of tangency which is where the onset of liquefaction occurs. We use $\frac{\partial \phi'}{\partial t'}$ constant in space except in the Fiegel and Kutter example (figure 4) where it is near constant in the sand and drops rapidly to zero in a manner similar to but slightly below the permeability transition so that there is no appreciable contraction of the silt itself. Since heating was earlier determined to be a small perturbation for sands we ignore it here for simplicity except in the example involving thermal liquefaction in silts. Also, we set $\beta(\hat{\phi}) = \hat{\phi} = 1$ and ignore the small effect of spatial variability in ϕ except as it influences k_d which is spatially varying as shown in each figure. By adjusting the characteristics of the soil, especially the permeability field and the spatial variation in the forcing, we can determine how the permeability and permeability gradient affect the onset of liquefaction. In some simple situations we can get a closed form solution to the resulting pressure field, and then we can examine the residual error with compressibility and heating effects, to determine where or when compressibility or heating might be important. In example situations where regions of space have low permeability such as $k_{d0}/20$ or less, a dynamic solution provides more details on the development of the pressure field, but an equilibrium solution can still provide great insight into the interplay between

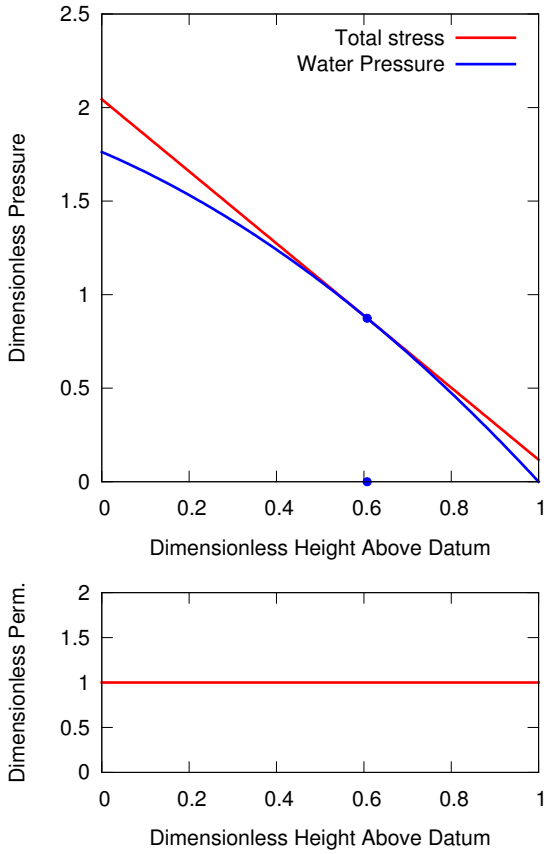

Figure 1: Parabolic water pressure is tangent to the linear total stress curve at the point of initial liquefaction in a uniform sand

regions of high and low permeability.

Uniform Loose Hydraulic Fill A model of a uniform loose hydraulic fill such as those found at reclaimed land in bays and port facilities worldwide would be a uniform deposit with $k'_d = 1$ of depth $z' \approx 1$. We assume for simplicity that the water table is at the surface of the ground, and we apply a 0.12 nondimensional pressure unit load on the ground designed to model 1/2 meter of concrete pad to ensure that the effective stress is not zero at the surface (figure 1). In this situation, due to the uniform permeability, the terms in the equation involving the spatial derivative of k_d disappear. If we assume the contractive forcing $\frac{\partial \phi'}{\partial t'}$ is constant in space and we are solving for equilibrium conditions, then the curvature of the pressure field is constant and we have a parabolic pressure curve.

In figure 1 we show the results of this simulation and we find that the soil just initiates liquefaction via loss of grain contacts at $z \approx 0.61$ when $\frac{\partial \phi'}{\partial t'} = -1.53$ corresponding to a ground surface velocity of $-0.08\,\mathrm{cm/s}$. For a 30 second earthquake and a 10 m deposit, this implies a vertical settlement of about 2.4 cm. Normally if the ground drops several centimeters we would see serious consequences for pipelines or structures on spread footings, and yet because the soil is so well drained, this loading just begins to initiate the total loss of contact between grains that is traditionally thought to be the hallmark of liquefaction. This example illustrates how sandy soil itself is quite well drained, and in this case it is actually because of this drainage that the settlement is possible. For looser or coarser soils, with permeabilities $k'_d > 4$ for example, the displacements could be catastrophic, a likely scenario for gravelly coarse sand fills.

Silty Inter-Layer Another case of interest is a simple model for the experiment of [6]. In this situation we have loose sandy soil with $k'_d = 1$ and a thin layer of much lower permeability $k'_d \sim .001$ with a large gradient in permeability around this minimum (see figure 2). Because of the large permeability gradients, there can be fast changing boundary layers in which the pressure gradients are high and develop over small regions so that the curvature of pressure is quite large. If we solve the steady state equation we find that with $\frac{\partial \phi'}{\partial t'} = -1.23$ the confining of pressure by the inter-layer forces a localized loss of grain contacts at $z' = 0.497$ just below the center of the layer. In the experiment of [6] there is the formation of a thin water film below the silt inter-layer in a manner consistent with these results.

In the follow up to those experiments [10], experiment 1 involves a silt inter-layer in a fine sand, in which a long-lasting stable layer of water below the layer was observed. This can be explained by the ratio of drag force to weight for small particles. If we consider a single spherical soil particle of radius R, the well known formula for Stokes drag is $f_d = -6\pi\mu R v$ [18] whereas the weight for a spherical grain is $w = \frac{4}{3}\pi R^3 \rho g$. If we take the fluid velocity to be the velocity in the water layer $v = \frac{k_d}{\mu}\frac{\partial P}{\partial z}$ the characteristic value of f_d/w for one nondimensional unit of each variable is therefore: $\frac{9k_{d0}}{2G_{gr}R^2}$. For sand grains with $R \sim 0.5$mm this ratio is 0.001 whereas for a silt grain with $R \sim 0.01$mm the ratio is 2.5 indicating that silt particles which fall down into the water layer are easily pushed back up by the drag caused by fluid flow whereas the sand will easily sink. In addition to this basic interpretation, [18] and [19] show that the drag on the particle increases dramatically as it integrates into the porous medium at the water-silt boundary so that once a layer is formed, the particles are unlikely to detach.

In their experiment 2 involving a fine sand overlying a coarse sand [10], a transitory turbulent water layer forms. This case can be understood in terms of the lack of a long-term strong gradient in pressure which would induce a large flow velocity comparable to the silt seam experiment, as well as a larger grain size in this experiment. Experiment 3 is similar to experiment 1 with grain sizes changed to be a fine sand inter-layer in a coarse sand. This exper-

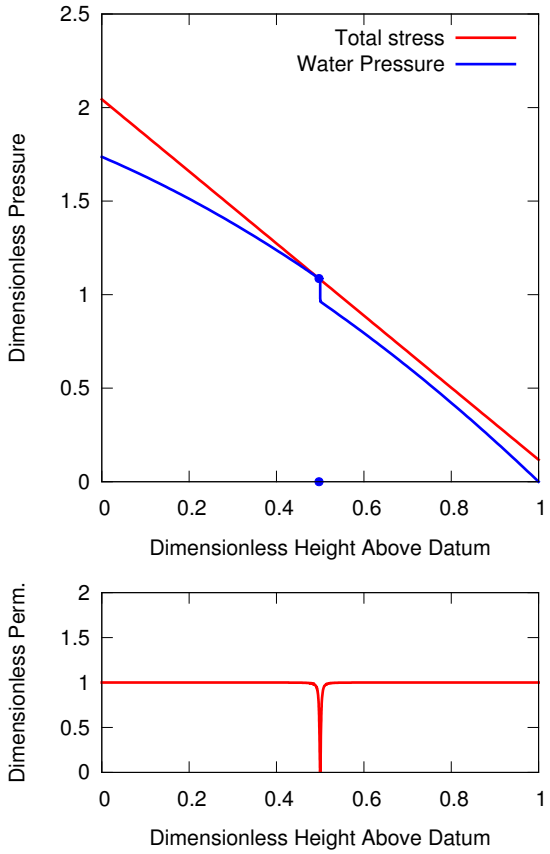

Figure 2: Silt layer embedded within loose sand. Liquefaction initiates below the region of lowest permeability where the large gradient in permeability induces a large second derivative of pressure, and a thin water film forms.

iment is substantially similar to experiment 1 with an altered timescale due to the different permeabilities involved. In experiment 4, the authors alter experiment 2 by making the upper fine sand layer unsaturated and the water layer is stabilized compared to experiment 2 [10]. The lack of water above the saturated-unsaturated interface means that the effective size of the upper fine sand layer is only 7 cm compared to 90 cm in model 2. This thinner upper layer means a larger pressure gradient can form and higher fluid velocities develop, thus higher drag develops on the upper sand particles which stabilizes the water film.

Liquefiable Sand Inter-Layer A typical warning sign for Geotechnical engineers is the existence of a loose sand layer between layers of denser and especially lower permeability material. This is the inverse of the silty inter-layer example

given above. When we make permeability $k'_d = 1/8$ outside of a region of width about 20cm (10 times as wide as the silty inter-layer) where permeability is 1 we find that the contraction of the deposit pushes water upwards out of the coarse sandy layer and the deposit liquefies in the fine sand above at $z' = 0.65$ with $\frac{\partial \phi'}{\partial t'} = -0.198$ which is *much* lower loading than in either the uniform or silty layer case (figure not shown). Due to the lower permeability of the main deposit, the diffusion is less dominant, and with less drainage, it is easier to cause liquefaction. This highlights the phenomenon that "drainage" is a non-local phenomenon which is affected by the entire permeability field. Sand itself may be locally well drained, but can be confined by low permeability boundaries. It also highlights the fact that within a tabletop apparatus, a sample of characteristic size in the range of 20 cm behaves in a way dominated by the boundary conditions of the apparatus, and not by the inherent properties of the material.

Fine-scale variability in permeability around an average value Due to the importance of permeability variation, we consider a model of a loose hydraulic fill sand whose layering structure causes a fine-scale oscillation in permeability of 30% about a typical value of $k'_d = 1$ (see figure 3). This oscillation occurs on a small length scale and is a simple model for variability in hydraulic fill material and the natural segregation of sandy soil by varying sinking rates due to varying grain sizes as pointed out by [10].

This example allows us to highlight the role of the variability in permeability. If the permeability field is $O(1)$ throughout, but has a fine scale oscillation of dimensionless length scale $\lambda \ll 1$ then the term $\frac{\partial k'_d}{\partial z'}$ becomes $O(1/\lambda)$ which can be quite large. To balance this we can either generate curvature of the pressure field to induce diffusion, or if diffusion is quenched by $k_d \frac{\partial^2 P'}{\partial z'^2} \sim 0$ then $(\frac{\partial P'}{\partial z'} + 1)$ must be $O(\lambda)$ to keep $\frac{\partial k'_d}{\partial z'}(\frac{\partial P'}{\partial z'} + 1) = O(1)$.

Suppose that a fine scale variation in P' develops so that $P' = F(z'/\lambda) + G(z')$ where F is an $O(1)$ function representing the fine scale variation and G is $O(1)$ representing the slow variation. Then $|\frac{\partial^2 P'}{\partial z'^2}| = O(1/\lambda^2)$ with a factor $1/\lambda$ coming from each derivative of F with respect to z'. In order for diffusion to be quenched we must have $k'_d \ll \lambda^2$. Since in real materials $0 < k'_d < O(1)$, necessarily the region where both $k'_d \ll \lambda^2$ and $|\frac{\partial k'_d}{\partial z'}| = O(1/\lambda)$ is extremely small. If k'_d is small, and the derivative of permeability is negative then it must become nonnegative quickly to keep $k'_d > 0$ or if the derivative is positive, k'_d increases rapidly so it does not remain small for long. This was seen in the thin layer example (figure 2), where in the region of rapidly changing k'_d we see curvature of the pressure field, and in the center of the layer where $k'_d \ll 1$ and $|\frac{\partial k'_d}{\partial z'}| \ll 1$ the large gradient in pressure develops so that $\frac{\partial k'_d}{\partial z'}(\frac{\partial P'}{\partial z'} + 1) = O(1)$ to balance the forcing.

If the overall size of k'_d is small everywhere, then we can rescale the k'_d variable everywhere, and by rescaling the t' variable the equation remains symmetric. This shows that for lower permeability soils an overall lower level of

forcing is required for liquefaction.

In the given example (figure 3), by using a Fourier series approach to approximate the analytical solution we see that the oscillations in permeability are completely dominated by the tendency for pressure diffusion in the equilibrium case so that the pressure field is nearly indistinguishable from the earlier constant permeability field and does not develop an important fine scale oscillation; in this example $\frac{\partial \phi'}{\partial t'} = -1.45$ and $z' = 0.599$ compared to the constant permeability model where $\frac{\partial \phi'}{\partial t'} = -1.53$ and $z \approx 0.61$.

Sand overlain by silt: A model for the experimental results of [5] In this model, a silt overlies a loose sand (figure 4). For this problem we have rescaled the z axis to correspond to the depth of the experiment and correspondingly rescaled pressure. Contractive forcing $\frac{\partial \phi'}{\partial t'}$ is spatially varying and appreciable only in the lower sand region. The water pressure curve is nearly linear in the silt which implies fluid flow at constant velocity. Clearly then, water is squeezed out of the lower sand and pressure diffuses into the upper silt, liquefying it at the base. Immediately after the end of shaking the experimental results qualitatively agree with this equilibrium solution. Failure occurs much later via a sand-boil which occurs presumably near a localized weakness within the silt layer. In our example, liquefaction occurs at $z' = 0.695$ which is slightly above the center of the permeability transition, which occurs at approximately 0.629. The required loading is $\frac{\partial \phi'}{\partial t'} = -0.524$ which has not been rescaled, and is significantly lower than in the uniform sand example (figure 1) where $\frac{\partial \phi'}{\partial t'} = -1.53$. The relatively thick silty layer makes drainage difficult and this contributes to a large reduction in the necessary loading.

Theoretical process of thermal liquefaction of silt By substituting $k'_d = \epsilon \hat{k}_d$ in the incompressible equation we can consider the case when typical permeability is small relative to sand, such as $\epsilon < .001$. When this is the case, diffusion does not act on the same time scale, and in fact the diffusion time scale $\Delta t/\epsilon > 140\,\mathrm{s}$ is larger than the typical duration of the earthquake. If a silt is somehow precluded from sustained grain skeleton contraction $\frac{\partial \phi'}{\partial t'}$, perhaps due to its initial porosity being near the equilibrium state, it could still theoretically liquefy by absorption of wave energy into thermal energy. The simplest case is a single homogeneous layer of silt similar to the homogeneous layer of sand above. Instead of contractive forcing, we apply $\frac{\partial S'}{\partial t'}$ and attempt to liquefy the silt via heating. The equation is similar to uniform contraction, and produces the same pressure field as figure 1. We find that the homogenous layer liquefies at $z' \approx 0.61$ when $\frac{\partial S'}{\partial t'} = 1.53\epsilon/\gamma_S$. The question arises then as to whether $\epsilon/\gamma_S = \mathrm{ord}(1)$ in some regimes of shaking and grain size so that silt might thermally liquefy by absorbing wave energy to heat. This is an interesting question for which a simple centrifuge experiment using a well insulated bucket and measuring before and after temperatures could give insight, or perhaps borehole measurements of thermal changes during an earthquake might be

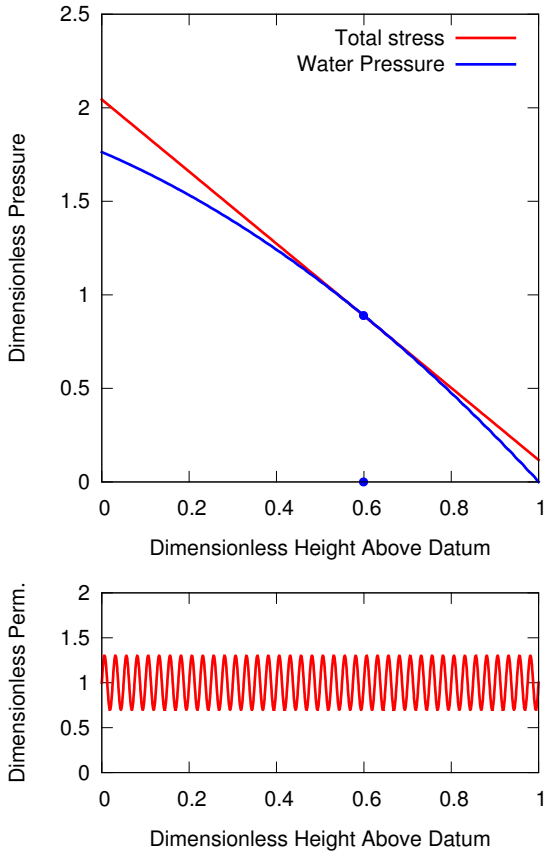

Figure 3: Liquefaction initiates at essentially the same place as in the constant permeability example despite a fine-scale oscillation in permeability of 30%. The dominant term in the differential equation is the $k'_d \frac{\partial^2 P'}{\partial z'^2}$ term so long as $k'_d \not\approx 0$ implying that large stable gradients in pressure do not form unless permeability becomes quite small as seen in the silt-layer example.

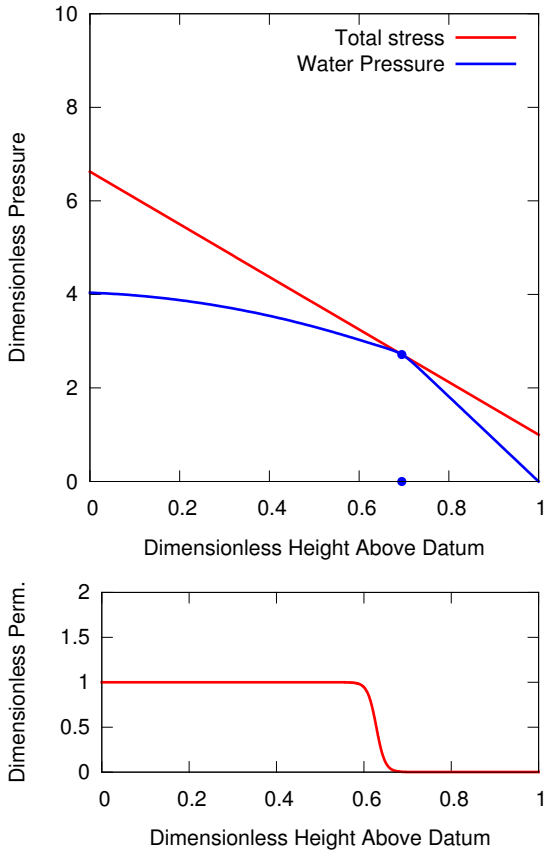

Figure 4: A model for the experimental results of [5] in which the step in permeability induces liquefaction at the sand-silt boundary where a sharp kink in pressure occurs. Here the spatial dimension has been rescaled by a factor $\epsilon \approx .34$ so that $z' \in [0, 1]$ corresponds to $z \in [0, 3.5]$ m, the dimensions of the experiment. Pressure and time have been rescaled by $\epsilon^2 \approx 0.12$ to maintain the order of magnitude of the coefficients in the equation.

available to provide insight.

Conclusions

By deriving a comprehensive equation for the water pressure development within layered soils and analyzing some critical examples we have shown that fluid flow driven by porosity changes and permeability changes is the main factor that causes pore pressure change during liquefaction. By comparison with experimental results [5, 6, 10] we show that sandy soil is well drained enough that it equilibriates on the same time scale as the earthquake. Also, due to our model of this drainage, we can identify several modes of liquefaction, from fluid flow induced "fast settlement" to localized water film formation at permeability boundaries, to flow induced liquefaction of low permeability layers that overly a high permeability layer, and even potentially thermally induced liquefaction when permeability is very low. In each of these example cases, we do not attempt to couple the behavior of the grains to the behavior of the water, or provide time-varying dynamic solutions, as no large scale continuum model is available for grain-fluid interaction behavior comparable in quality to the DEM model of [7].

Modeling a 1/4 m square cross section 10 meters long with 1mm diameter typical grain sizes would require perhaps 10^8 grains and be computationally prohibitive. However for qualitative understanding of the liquefaction process it is sufficient to perform a careful analytical analysis of a continuum model of water flow through soil driven by changes in pore volume. Our analysis provides tremendous insight without supercomputing requirements. We conclude several important things:

- Soil liquefaction in water saturated sands is a process caused by fluid flow due to gravitational pumping, not fluid stagnation in an "undrained" event. Thin regions of low permeability silt do not prevent drainage, as large pressure gradients will develop to force fluid through these layers. However, their presence significantly influences the location and ease of onset of liquefaction. Large regions of low permeability soil can significantly reduce drainage, leading to liquefaction at significantly lower rates of grain contraction.

- Due to water pressure diffusion, we can not examine the liquefaction process by simply considering local properties of soil in a small sample on a tabletop apparatus, given the characteristic length scales of ord(10) meters, and corresponding characteristic time scales of tenths of seconds. Therefore, geotechnical centrifuge experiments are the only meaningful physical experiments for this phenomenon.

- In lower permeability materials such as thick regions of fine sand or silt, the time scales for the water flow process can be longer. For an earthquake duration of 30 s, the duration is not small compared to the water flow

characteristic time until the characteristic time is significantly longer than we use here. But these long equilibriation times occur when the typical permeability throughout the material is $O(10^{-13})\,m^2$ which is well below the sandy range [14]. It is an interesting question as to whether, in large deposits of silt, liquefaction damage will occur in undrained conditions or whether in practice fluid flow is necessary. Liquefaction of pure silty soils is not a frequently observed condition, and this suggests that in most cases fluid flow is important.

- Impedance to flow caused by local sharp reductions in permeability is the main driving force in localized liquefaction events, and can cause the formation of water films that lubricate layers of soil allowing large lateral spreading. For level ground, failure is expected via localized sand boils at fissures, or the liquefaction of overlying layers as fluid flow stagnates. This phenomenon can only be explained by explicitly acknowledging the flow of water.

- "Liquefaction" as the term is commonly used is not necessarily associated with total loss of effective stress. Large settlements could occur without the formation of a fully liquefied layer if loose soil settles while water flows to the surface.

- In silts, where permeability is small and diffusion can not act on the earthquake duration timescale, extensive shaking might concievably cause liquefaction through heating effects, a previously unexplored phenomenon.

References

[1] Sawicki A, Mierczyski J. Developments in Modeling Liquefaction of Granular Soils, Caused by Cyclic Loads. Applied Mechanics Reviews. 2006;59(2):91. Available from: `http://link.aip.org/link/AMREAD/v59/i2/p91/s1\&Agg=doi`.

[2] Kramer S. Geotechnical earthquake engineering. Upper Saddle River N.J.: Prentice Hall; 1996.

[3] Holtz R, Kovacs W. An introduction to geotechnical engineering. Englewood Cliffs N.J.: Prentice-Hall; 1981.

[4] Sivathayalan S, Vaid Y. Truly undrained response of granular soils with no membrane-penetration effects. Canadian Geotechnical Journal. 1998;35(5):730–739. Available from: `http://www.nrc.ca/cgi-bin/cisti/journals/rp/rp2\_abst\_e?cgj\_t98-048\_35\_ns\_nf\_cgj35-98`.

[5] Fiegel GL, Kutter BL. Liquefaction Mechanism for Layered Soils. Journal of Geotechnical Engineering. 1994;120(4):737. Available from: `http://link.aip.org/link/JGENDZ/v120/i4/p737/s1\&Agg=doi`.

[6] Kokusho T. Water Film in Liquefied Sand and Its Effect on Lateral Spread. Journal of Geotechnical and Geoenvironmental Engineering. 1999;125(10):817. Available from: http://link.aip.org/link/JGGEFK/v125/i10/p817/s1\&Agg=doi.

[7] Goren L, Aharonov E, Sparks D, Toussaint R. The Mechanical Coupling of Fluid-Filled Granular Material Under Shear. Pure and Applied Geophysics. 2011 Jun;Available from: http://www.springerlink.com/index/10.1007/s00024-011-0320-4.

[8] Goren L, Aharonov E, Sparks D, Toussaint R. Pore pressure evolution in deforming granular material: A general formulation and the infinitely stiff approximation. J Geophys Res. 2010;115.

[9] Fowler A. Mathematical models in the applied sciences. (Repr.) ed. Cambridge: Cambridge Univ. Press; 1998.

[10] Kokusho T, Kojima T. Mechanism for Postliquefaction Water Film Generation in Layered Sand. Journal of Geotechnical and Geoenvironmental Engineering. 2002 Feb;128(2):129–137. Available from: http://link.aip.org/link/?QGT/128/129/1.

[11] Idriss IM, Boulanger RW. Semi-empirical procedures for evaluating liquefaction potential during earthquakes. Soil Dynamics and Earthquake Engineering. 2006;26(2-4):115130.

[12] Seed R, Cetin K, Moss R, Kammerer A, Wu J, Pestana J, et al. Recent advances in soil liquefaction engineering: a unified and consistent framework. In: Proceedings of the 26th Annual ASCE Los Angeles Geotechnical Spring Seminar: Long Beach, CA; 2003. .

[13] The Maxima Project. Maxima, A Computer Algebra System. Version 5.29.1 http://maxima.sourceforge.net.; 2013. Available from: http://maxima.sourceforge.net.

[14] Beard D, Weyl P. Influence of Texture on Porosity and Permeability of Unconsolidated Sand. AAPG Bulletin. 1973;57. Available from: http://search.datapages.com/data/doi/10.1306/819A4272-16C5-11D7-8645000102C1865D.

[15] Nemat-Nasser S, Shokooh A. A unified approach to densification and liquefaction of cohesionless sand in cyclic shearing. Canadian Geotechnical Journal. 1979;16(4):659–678. Available from: http://www.nrc.ca/cgi-bin/cisti/journals/rp/rp2_abst_e?cgj_t79-076_16_ns_nf_cgj16-79.

[16] Davis RO, Berrill JB. Pore Pressure and Dissipated Energy in EarthquakesField Verification. Journal of Geotechnical and Geoenvironmental Engineering. 2001;127(3):269. Available from: http://link.aip.org/link/JGGEFK/v127/i3/p269/s1\&Agg=doi.

[17] NIST. Thermophysical Properties of Fluid Systems; 2013. http://webbook.nist.gov/chemistry/fluid/. Available from: http://webbook.nist.gov/chemistry/fluid/.

[18] Brinkman HC. A calculation of the viscous force exerted by a flowing fluid on a dense swarm of particles. Applied Scientific Research. 1949 Dec;1:27–34. Available from: http://www.springerlink.com/index/10.1007/BF02120313.

[19] Verschoor H. Experimental data on the viscous force exerted by a flowing fluid on a dense swarm of particles. Applied Scientific Research. 1951 Jan;2:155–161. Available from: http://www.springerlink.com/index/10.1007/BF00411979.